Stellar Rotation
Proceedings IAU Symposium No. 215, © 2003 IAU
André Maeder & Philippe Eenens, eds.

Multidimensional Hydrodynamic and Hydrostatic Stellar Models

Robert G. Deupree

Dynamic Experimentation Division, Los Alamos National Laboratory, Los Alamos, NM, 87545 USA and Institute for Computational Astrophysics, St. Mary's University, Halifax, Nova Scotia, Canada

Abstract. Results for multidimensional stellar model simulations of both 2D and 3D hydrodynamic models and 2D stellar evolution sequences are presented. Simulations of the highly superadiabatic region of the solar convective region provide a good example of the current status and limitations of explicit 3D finite difference methods in stellar problems. Such simulations cannot be used for stellar cores, where the motion is expected to be well subsonic. The results of some 2D fully implcit hydrodynamic simulations of convective cores and shells are given for models with and without rotation, and their effects examined through fully 2D stellar evolution sequences. One effect of moderate to rapid rotation in convective cores is to alter the convective flow pattern so that convective eddies tend to line up parallel to the rotation axis. Rotation also appears to modestly reduce the amount of convective core overshooting, at least for intermediate mass models.

1. Introduction

Multidimensional explorations of stars have become increasingly common over the last few years. While perhaps not routine, they are becoming at least sufficiently numerous to play an increasingly important part in stellar studies. An obvious application is the 3D explicit finite difference technique simulation of the upper region of the solar convection zone where the temperature gradient is expected to be significantly superadiabatic. The assumptions and results of two papers will be examined which represent the current capabilities and limitations of this approach. The explicit nature of these calculations effectively restricts their use to situations in which the flow speeds are some reasonable fraction of the sound speed. This is unlikely to be true for treating convection in stellar interiors, and one must either use implicit methods or approaches like the anelastic modal approximation (e.g., Ogura & Phillips 1962, Latour, et al. 1976, Gilman & Glatzmaier 1981). For stellar interiors I present some results of 2D fully implicit, finite difference simulations of convective cores and shells, with and without rotation, and the effects of the results of these simulations on stellar evolution through 2D stellar evolution calculations.

https://doi.org/10.1017/S0074180900195919 Published online by Cambridge University Press

2. 3D Simulations of the Top of the Solar Convection Zone

The current state of the numerical art in the arena of 3D finite difference simulations of quiescient stellar models may perhaps be represented by two recent papers on the superadiabatic region of the solar convection zone by Robinson, et al. (2003) and Asplund, et al. (2000). These calculations use on the order of 10^5 zones. This may be compared with the largest calculation of which I am aware (in another field) that has nearly 10^9 zones. This latter number suggests what zoning capabilities astrophysics can expect to have available in the next few years.

These calculations simulate only the upper part of the convective region where the velocities are a reasonable fraction of the sound speed. They are also limited in the horizontal width of the problem (usually with a ratio of width to depth of about 2.5), so that the convective region simulated is a box which includes only a very small fraction of the solar convection zone. The small size means that this is not a suitable vehicle to study the effects of rotation on the flow (this is not to suggest that rotation was a consideration for the authors). Periodic boundary conditions are assumed on the sides of the box.

The turbulence model used in stellar convection studies is nearly always a variant of the Smagorinsky (1963) analytic expression for the eddy viscosity. It has the virtue that it is simple, both in concept and application. Other models are available, but they are generally more complicated, such as solving a differential equation for the turbulent kinetic energy density at each mesh point to obtain an eddy viscosity coefficient which can vary in space and time. There are some modest differences between turbulence models, with the extent of convective overshooting being one, at least for the core helium flash (Deupree 1996). One reason why the results for different turbulence models are fairly similar is that they are nearly all have the same baseline sets of laboratory or environmental data which are used to determine the values of the free parameters. It is not clear that our knowledge of stellar convection is sufficient to justify one turbulence model over another, and most researches have chosen to keep the model as simple as possible.

A number of numerical issues are examined in one or both papers. The effects of the upper and lower zero velocity boundary conditions used by Robinson, et al. appear to limited to the region near the boundary, at least if the lower boundary is sufficiently deep. Asplund, et al. allow the velocity to be nonzero at the vertical boundaries and the relatively modest velocity differences near the vertical boundaries between the two papers tend to support this conclusion. The ratio of width to depth, generally taken to be 2.5 appears to provide satisfactory resolution of horizontal variables, although the two papers seem to disagree the sensitivity of the velocities to the horizontal resolution. While it seems like there are a number of details to be worked out, current computational capabilities are sufficient to allow a reasonable number of models to be calculated to cover the variety of numerical issues which need to be resolved.

https://doi.org/10.1017/S0074180900195919 Published online by Cambridge University Press

3. 2D Interior Hydrodynamic and Stellar Evolution Studies

Here I first summarize the results of a number of 2D ZAMS convective core hydrodynamic simulations, with and without rotation, by Deupree (2000, 2001). These calculations have been performed for masses between 3 and 20 $M_\odot$ for both rotating and nonrotating models. The 2D rotation is expressed by the ratio of the surface polar radius to the surface equatorial radius, and the values used were 1, 0. 98, 0.93, 0.84, and 0.72. These values cover a wide range or rotation rates, but stop somewhat short of critical rotation. For a 20 $M_\odot$ model, these ratios of the surface polar to surface equatorial radius correspond to surface equatorial velocities of 0, 150, 300, 450, and 600 km s^{-1}. Critical rotation for this model occurs at a surface equatorial velocity of about 750 km s^{-1}.

The results of the hydrodynamic simulations of the convective cores of these models may be summarized as follows: 1) the flow velocities in the convective cores are appreciably higher than the standard phenomenological models would predict (tens of km s^{-1} versus hundreds of m s^{-1}, 2) as a consequence of this, at any given time we may have both highly superadiabatic and subadiabatic gradients in the core, although the average over space and time is adiabatic to within computational accuracy, 3) there is appreciable overshooting beyond the boundary of the convective core as measured by the motion of tracer particles, more at higher mass (about 0.6 H_p at 20 $M_\odot$ versus 0.25 H_p for 2 $M_\odot$) and less for increasing rotation, at least for lower mass models (by about 0.15 H_p between a nonrotating model and the most rapidly rotating model), 4) the convective eddies tend to become oriented parallel to the rotation axis rather than vertically for moderate and rapid rotation, and 5) the distribution of the rotation rate in the convective core is neither uniform nor constant angular momentum per unit mass, but can be represented by a power law in the distance from the rotation axis (less reasonably for slow rotation than for rapid rotation) with an exponent of approximately -0.5.

Based on these results I have performed several 2D stellar evolution sequences of nonrotating and rotating models. The first of these was a nonrotating sequence designed to be compared with the standard calculations of 1D stellar evolution codes. This sequence was carried into core helium burning and was terminated at a central helium abundance of about 0.8 where my lack of inclusion of carbon as a composition variable begins to affect the nuclear burning. This calculation was compared with the Brunish & Truran (1982a,b) version of the Iben (1963, 1965a, b) code with updated physics, a relatively current (mid 2000) version of the Paczynski (1970) code, and with the Yale evolutionary code YREC (Guenther & Demarque 1997, 2000). No attempt has been made to make the equation of state and nuclear reaction rates of all codes common, but they all do have the OPAL opacities (Iglesias & Rogers 1996). Rather than try to alter some of the other codes, I have performed all calculations without convective core overshooting.

The agreement among the four codes was quite good through core hydrogen burning and the early stages of hydrogen shell burning. At this point, both the Paczynski code and YREC stopped because they ran out of the physical input tables. Significant effort would be required to allow these codes to continue to later phases with the same physical input. The comparison with the Iben code

https://doi.org/10.1017/S0074180900195919 Published online by Cambridge University Press

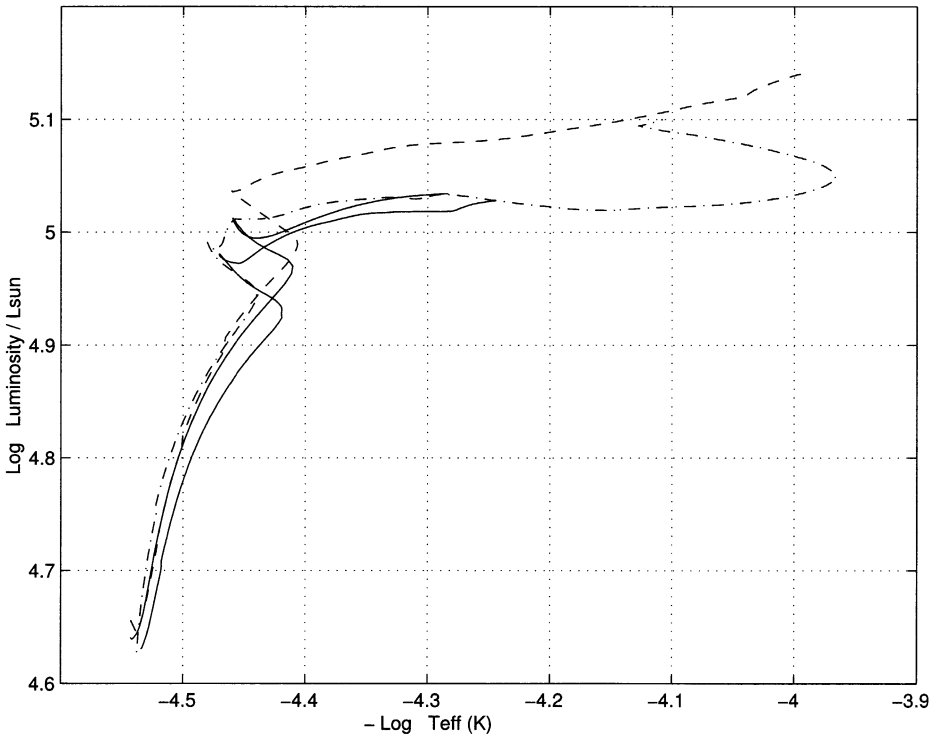

Figure 1. Comparison of the evolutionary tracks for a 20 $M_\odot$ model calculated with the Paczynski code (upper solid curve), YREC (lower solid curve), the Iben code (dashed curve), and the 2D code ROTORC (dot-dash curve).

was carried on into core helium burning. The evolutionary tracks for all four models are shown in Figure 1.

There is an interesting difference between the Iben code (and I expect it would be true for the other codes as well) and the 2D code at relatively late time in hydrogen shell burning. This arises from the fact that the velocities must be calculated in the 2D code because it is not a Lagrangian code and the velocities are needed to determine where the individual zones go with respect to the mesh. The velocity terms are relatively large here (about 0.2 cm s^{-1} as the model crosses an effective temperature of about 13000K), and they do not disappear instantaneously with the helium core ignition. This results in the loop to the right in the HR diagram in the 2D evolution track in Figure 1. The time scale for the loop is short, but not extremely so (68000 yr between the times when the effective temperatures are the same and equal to the value at the left end of the loop where quiescent core helium burning starts), and the model settles down into core helium burning at essentially the same place in the HR diagram as the Iben code does. The luminosity increase from the red end of the loop to the blue end where core helium burning is well underway reflects the gradual cessation of the use of the radiation emerging from the hydrogen burning shell to

https://doi.org/10.1017/S0074180900195919 Published online by Cambridge University Press

drive the envelope expansion. Note that this loop has nothing to do with the 2D nature of the calculation, but only on the inclusion of the acceleration terms in the momentum equation and the work terms in the energy equation. The effect is fairly large here because the velocities are fairly large. They are much smaller for lower mass models and for models which begin core helium burning closer to the main sequence. Based on a detailed comparison with the Iben results, I feel fairly confident that the 2D code functions well as an evolutionary code with the traditional assumptions.

Even though the calculation does not include rotational mixing of any sort, I was unable to resist the temptation to run the rapidly rotating model as a "standard" evolutionary calculation to see if anything interesting occurred. One of the standard features is uniform mixing in convective regions defined by the Schwarzschild criterion, and it was found that the convective region associated with the hydrogen burning shell that forms at this mass is very aspherical. The Schwarzschild formal boundaries of the convective regions at one time during core helium burning are shown in Figure 2. The helium burning convective core is highly oblate, as one might expect for a rapidly rotating model, but the hydrogen shell burning convective core is much larger at the equator than at the poles. This at least suggests that the convective criteria deserve thoughtful consideration.

One other feature of this model worth noting is that the differences between nonrotating and rotating models at the model center (lower central temperature and higher central density for rotating models) are present at core helium burning, but with larger differences than on the ZAMS. For example, the central temperatures for the nonrotating and rotating ZAMS models are 3.548×10^7K and 3.499×10^7K, respectively, while for core helium burning with Y=0.95 the temperatures are 1.703×10^8K and 1.570×10^8K, respectively. This means that quiescent core helium burning starts at an appreciably lower temperature and higher density for the rotating model, which may change the relative abundances of carbon and higher elements by the end of core helium burning in rapidly rotating models with respect to the abundances for nonrotating models.

With these issues in mind, I decided to explore the hydrogen shell convective region. This is of particular interest since the convective region forms where there is a composition gradient and thus we may learn something about the relatively applicability of the Schwarzschild criterion versus the Ledoux criterion. Here I calculated evolution sequences with overshooting and the power law representation of the rotational velocity based on the hydrodynamic simulations of the ZAMS convective cores. However, there is no special rotational mixing or mass loss. Starting from the ZAMS models, I evolved 20 $M_\odot$ models into hydrogen shell burning. During core hydrogen burning I performed several hydrodynamic simulations to see if the convective core overshooting and angular momentum distribution changed, but the results indicated that such changes were small.

Turning to the nonrotating model first, I performed a hydrodynamic simulation of a model just prior to the onset of convective instability (by either the Schwarzschild or Ledoux criterion). As expected, the model produced no significant hydrodynamic motion. The next model for which I took a dump had eleven radial zones (zones 137-148) unstable according to the Schwarzschild criterion,

https://doi.org/10.1017/S0074180900195919 Published online by Cambridge University Press

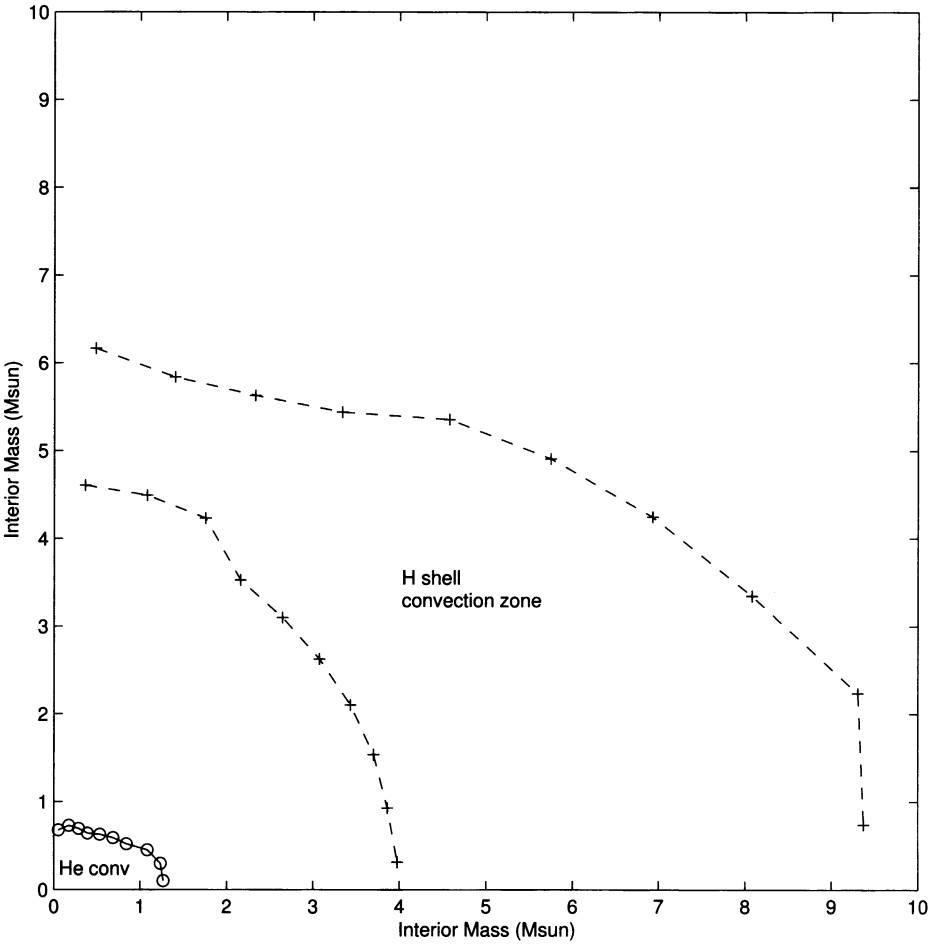

Figure 2. Formal boundaries defined by the Schwarzschild criterion of the He burning convective core and the convective region associated with the hydrogen burning shell for a rapidly rotating 20 $M_\odot$ 2D model using traditional 1D stellar evolution model assumptions. The radial variable is the interior mass, converted from the fractional surface equatorial radius using the horizontal average of the density. The polar direction is vertical and the equatorial direction horizontal. The He burning convective core is highly oblate, as one might expect from its rapid rotation. The convective region associated with hydrogen shell burning is highly aspherical, indicating perhaps that the treatment of the convective boundaries should be investigated carefully for models with rotation.

https://doi.org/10.1017/S0074180900195919 Published online by Cambridge University Press

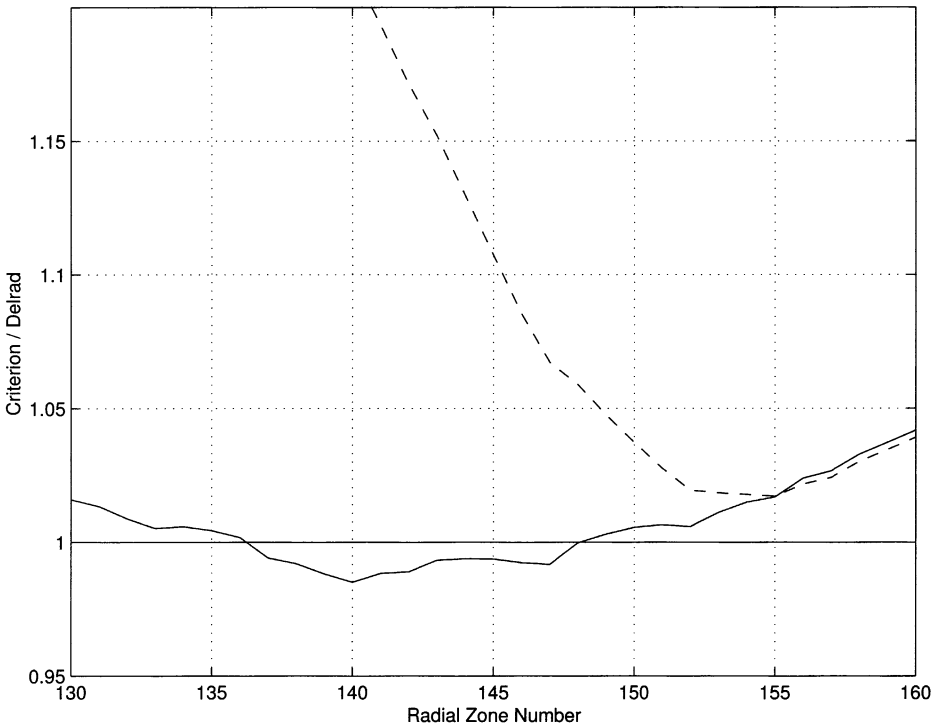

Figure 3. Ratio of the convective stability criterion to the radiative gradient as a function of radial zone number for the first model in the evolutionary sequence with a convectively unstable shell as determined by the Schwarzschild criterion. A ratio less than unity implies convective instability. The solid curve results from the Schwarzschild criterion and the dash from the Ledoux criterion. There are eleven radial zones which are modestly unstable according to the Schwarzschild criterion and none according to the Ledoux criterion. The hydrodynamic simulation shows modest convective activity and complete mixing in the upper part of the Schwarzschild defined convective region.

and no zones unstable according to the Ledoux criterion, as shown in Figure 3. Here the hydrodynamic calculation showed appreciable motion in the upper part (radial zones 145-148) of the Schwarzschild defined convective region, but much less in the lower part where the composition gradient is steeper. This calculation was followed for about ten days. After about three days the composition in the upper part of the convective region had become nearly uniform, while that below was only slightly modified. This composition profile was maintained with only very minor modifications throughout the remaining seven days of the calculation. I compare the beginning composition profile with the horizontal average of the composition at the end of the calculation in Figure 4.

Based on this result I allowed the upper part of the convection zone to mix and the lower part to be unmixed as an initial model for continuing the stellar evolution sequence. The Schwarzschild formal boundaries of the convective region grow as the evolution continues. Hydrodynamic simulations of later

https://doi.org/10.1017/S0074180900195919 Published online by Cambridge University Press

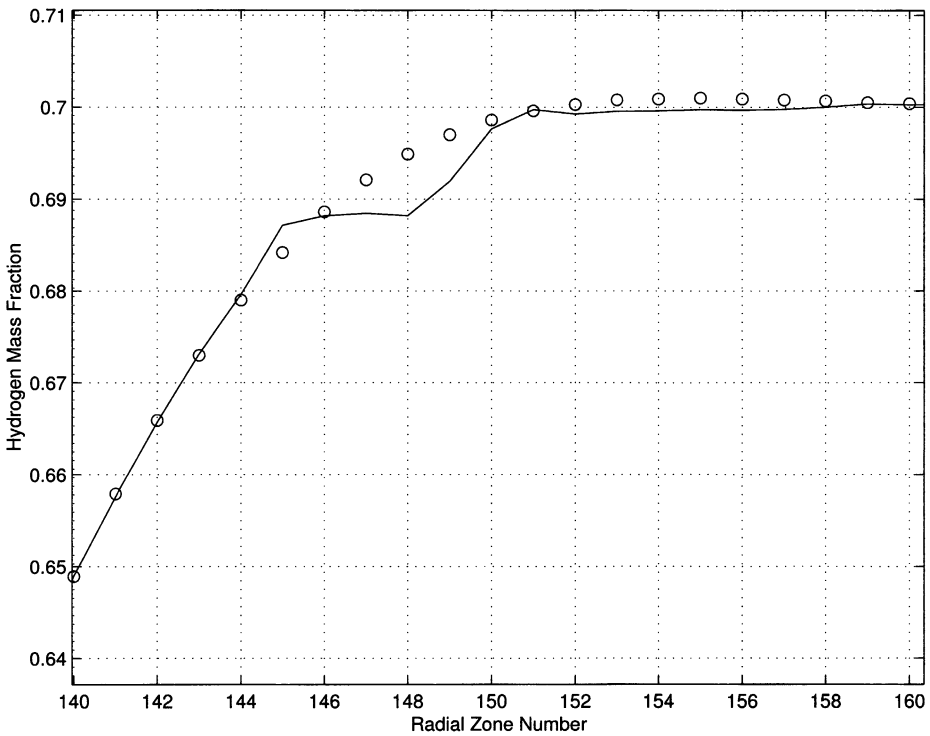

Figure 4. Hydrogen mass fraction as a function of radial zone number. The circles denote the values for the hydrostatic model that was used to begin the hydrodynamic simulations, and the solid curve represents the horizontal average of the hydrogen mass fraction for the last hydrodynamic model at ten days after the beginning of the simulation (although the differences in the horizontal average are very slight after three days). The Schwarzschild defined convective region is between radial zones 137 and 148. In the upper part of the Schwarzschild defined convective region (radial zones 145-148) the composition has become effectively uniform, with the necessary steepening of the composition gradient to match the values at distant locations from the uniformly mixed region. There has been little modification to the composition in the lower part of the Schwarzschild defined convective region.

https://doi.org/10.1017/S0074180900195919 Published online by Cambridge University Press

evolutionary models continue to show that the upper region of the convective region mixes, but that the lower region does not, at least on the time scale of the hydrodynamic simulations.

I also calculated the companion evolutionary sequence for a rapidly rotating model. The primary effect is that the convective region forms later in the hydrogen shell burning phase and is smaller than for the nonrotating model. This is most likely due to the smaller "effective g" for the rotating model and the fact that the convection zone is smaller for lower masses. The convective region is aspherical, being smaller at the pole than at the equator. In the associated hydrodynamic simulations, the tracer particles near the equator cover more ground than those near the pole, but there is some slight tendency of the tracer particles at the bottom of the convection zone to penetrate the bottom of the convective region horizontally. Figure 5 shows the motion of a number of tracer particles in the two dimensional grid. It is quite clear that the motion near the pole is appreciably less, as determined by the length of the individual traces, than it is near the equator.

These calculations are in a fairly early stage of refinement. A number of other features need to be included, most notably following secular instabilities which allow material to be mixed. These simulations are sufficient to reveal that there is a possibility for a richness in solution space which 1D models of rotation do not capture. Further work is required to determine if this is truly the case.

References

Asplund, M., Ludwig, H.-G., Nordlund, A., & Stein, R. F. 2000, A&A 359, 669.

Brunish, W. M. & Truran, J. W. 1982a, ApJ 256, 247.

Brunish, W. M. & Truran, J. W. 1982b, ApJS 49, 447.

Deupree, R. G. 1996, ApJ 471, 377.

Deupree, R. G. 2000, ApJ 543, 395.

Deupree, R. G. 2001, ApJ 552, 268.

Gilman, P. A. & Glatzmaier, G. A. 1981, ApJS 45, 335.

Guenther, D. B. & Demarque, P. 1997, ApJ 484, 937.

Guenther, D. B. & Demarque, P. 2000, ApJ 531, 503.

Iben, I., Jr. 1963, ApJ 138, 452.

Iben, I., Jr. 1965a, ApJ 141, 993.

Iben, I., Jr. 1965b, ApJ 142, 1447.

Iglesias, C. A. & Rogers, R. J. 1996, ApJ 464, 943.

Latour, J., Spiegel, E. A., Toomre, J. & Zahn, J.-P. 1976, ApJ 207, 233.

Ogura, Y. & Phillips, N. A. 1962, J. Atmos. Sci. 19, 173.

Paczynski, B. 1970, ActaAstron. 20, 47.

Robinson, F. J., Demarque, P., Li, L. H., Sofia, S., Kim, Y.-C., Chan, K. L. & Guenther, D. B. 2003, MNRAS 340, 923

Smagorinsky, J. 1963, Mon. Weather Rev. 91, 99.

https://doi.org/10.1017/S0074180900195919 Published online by Cambridge University Press

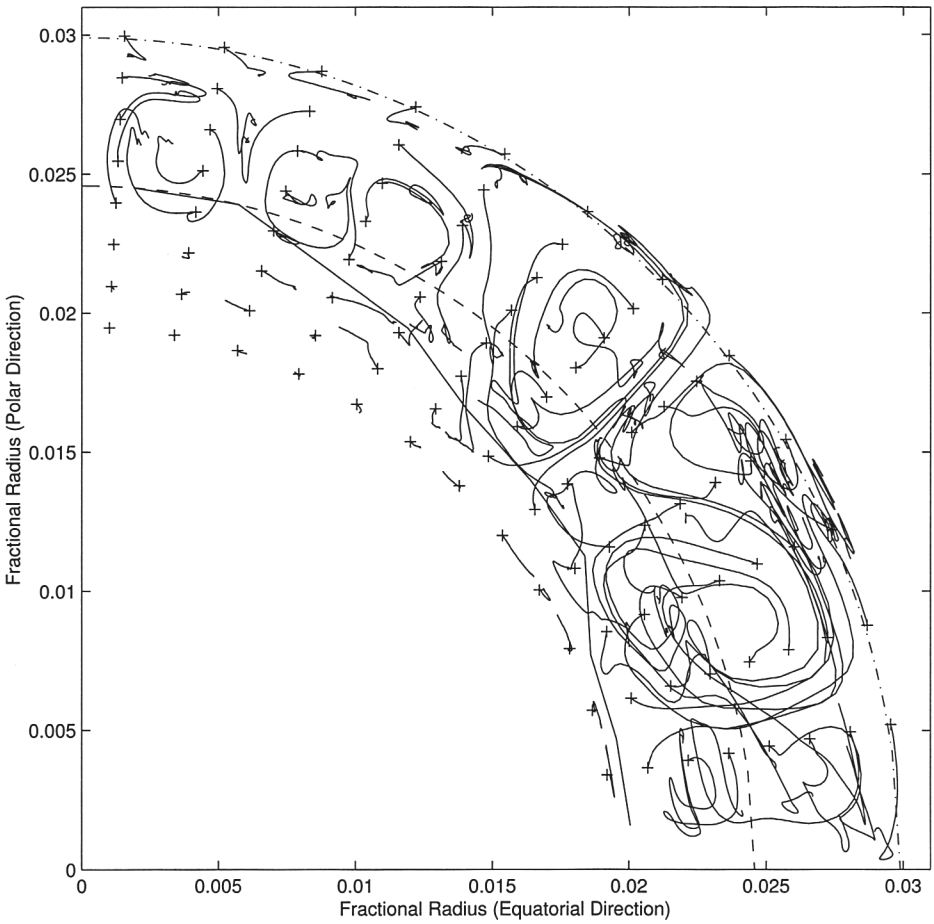

Figure 5. Motion of tracer particles in the convective region associated with hydrogen shell burning for a rapidly rotating 20 $M_\odot$ model. The static model occurs in the evolution some time after the convective region has formed. Each tracer particle begins at a plus sign. The dash-dot curve denotes the outer boundary of the mixed region in the static model. This includes some overshooting. The solid curve denotes the formal inner boundary of the convective region as determined by the Schwarzschild criterion. The dash curve represents a spherical surface at the formal convective boundary innner radius at the pole. Note the difference in motion between low and high latitudes.

https://doi.org/10.1017/S0074180900195919 Published online by Cambridge University Press